HHS Public Access

Author manuscript

J Immunol. Author manuscript; available in PMC 2017 June 15.

Published in final edited form as:

J Immunol. 2016 June 15; 196(12): 5089–5100. doi:10.4049/jimmunol.1502270.

Correction of MFG-E8 resolves inflammation and promotes cutaneous wound healing in diabetes

Amitava Das[*], **Subhadip Ghatak**[*], **Mithun Sinha**[*], **Scott Chaffee**[*], **Noha S. Ahmed**, **Narasimham L. Parinandi**[†], **Eric S. Wohleb**[‡], **John F. Sheridan**[‡], **Chandan K. Sen**[*], and **Sashwati Roy**[*]

[*]Departments of Surgery, Davis Heart and Lung Research Institute, Center for Regenerative Medicine and Cell Based Therapies and Comprehensive Wound Center, The Ohio State University Wexner Medical Center

[†]Department of Internal Medicine, The Ohio State University Wexner Medical Center

[‡]Division of Biosciences, The Ohio State University, Columbus, Ohio 43210

Abstract

Milk fat globule EGF factor 8 (MFG-E8) is a peripheral glycoprotein which acts as a bridging molecule between the macrophage and apoptotic cells thus executing a pivotal role in the scavenging of apoptotic cells from affected tissue. We have previously reported that apoptotic cell clearance activity or efferocytosis is compromised in diabetic wound macrophages. In this work we test the hypothesis that MFG-E8 helps resolve inflammation, supports angiogenesis and accelerates wound closure. MFG-E8$^{-/-}$ mice, displayed impaired efferocytosis associated with exaggerated inflammatory response, poor angiogenesis and wound closure. Wound macrophage-derived MFG-E8 was recognized as a critical driver of wound angiogenesis. Transplantation of MFG-E8$^{-/-}$ bone marrow to MFG-E8$^{+/+}$ mice resulted in impaired wound closure and compromised wound vascularization. On the other hand, MFG-E8$^{-/-}$ mice that received wild-type bone marrow showed improved wound closure and improved wound vascularization. Hyperglycemia and exposure to advanced glycated end products inactivated MFG-E8 recognizing a key mechanism that complicates diabetic wound healing. Diabetic db/db mice suffered from impaired efferocytosis accompanied with persistent inflammation and slow wound closure. Topical rMFG-E8 induced resolution of wound inflammation, improvements in angiogenesis and acceleration of closure upholding the potential of MFG-E8 directed therapeutics in diabetic wound care.

Introduction

Diabetic ulcer is a serious complication associated with type 2 diabetes mellitus (T2DM) (1-2). A chronic inflammatory state is a characteristic feature of these ulcers (3-4). Inflammation, an integral component of wound repair, defends against invading microbes

Address correspondence to: Sashwati Roy, PhD, 473 West 12th Avenue, 511 DHLRI, The Ohio State University Medical Center, Columbus, Ohio 43210, Phone: (001)-614-247-7657, Fax: (001)-614- 247- 7818, sashwati.roy@osumc.edu.

Disclosures. The authors have no financial conflicts of interests.

and supports tissue repair through delivery of healing factors by blood-borne cells (5). Resolution of inflammation is a dynamically regulated process the timeliness of which has major bearing on healing outcomes. Such critical process is subject to refined control by a multitude of factors including cytokines, chemokines, and lipid mediators (6). Previous work by our laboratory demonstrated that under conditions of diabetes, resolution of wound inflammation is challenged by several barriers (7). For example, diabetic wounds suffer from impaired engulfment of apoptotic cells by mϕ resulting in increased apoptotic cell burden at the wound site. As a result, resolution of wound inflammation is derailed complicating healing outcomes (7).

Macrophages (mϕ) are major contributors to cutaneous wound healing (8-9). At the wound-site, successful efferocytosis by mϕ achieves cleansing and resolution of inflammation (10-13). Milk fat globule-epidermal growth factor (EGF)-factor VIII (MFG-E8) is a secreted glycoprotein protein that promotes efferocytosis by bridging apoptotic cells on phagocytes with mϕ (14-15). MFG-E8 contains two EGF domains, a proline/threonine-rich domain, and two factor-VIII-homologous domains (15). Mϕ derived MFG-E8 specifically binds apoptotic cells by recognizing aminophospholipids such as phosphatidylserine. While engaged by phosphatidylserine on apoptotic cells, MFG-E8 binds to dying cells particularly to integrin αvβ3 and αvβ5 *via* its RGD (arginine-glycine-aspartate) motif (15-16). In addition to its critical role in efferocytosis, MGF-E8 possesses known pro-angiogenic effect supporting VEGF function in adult neovascularization (16). Consistently, recombinant MFG-E8 treatment improve wound angiogenesis (17). However, questions addressing the primary source of MFG-E8 *in vivo* and the mechanistic underpinnings that determine the significance of MFG-E8 at the wound site remain open. In this work, we sought to characterize the mechanisms by which mϕ-derived MFG-E8 regulates wound inflammation.

Materials & Methods

Human subjects and fluid collection from chronic wounds

Subjects participating in the study were chronic wound patients seen at The Ohio State University Comprehensive Wound Center clinics and have been undergoing negative pressure wound therapy (NPWT) as part of standard clinical care. Demographic characteristics of patients and wound-related information are presented in Table 1. The NPWT dressing (sponges) were collected from each patient for cell isolation and wound fluid collection. Wound fluids were derived from NPWT dressing by lavaging the wound dressing with saline solution (18). All human studies were approved by The Ohio State University Institutional Review Board. Declaration of Helsinki protocols was followed, and patients gave their written informed consent.

Secondary Intention Excisional Murine Dermal Wound Model

Male C57BL/6 mice (age, 8–10 weeks old) were obtained from Harlan Laboratory. Mice homozygous for spontaneous mutation of the leptin receptor ($Lepr^{db}$) (BKS.Cg-$m^{+/+}$ $Lepr^{db/J,}$ or db/db; stock no 000642) and their respective non-diabetic lean control littermates (db/+) were procured from Jackson laboratories. B6.129(Cg)-$Gt(ROSA)26Sor^{tm4(ACTB-tdTomato,-EGFP)Luo}$/J mice obtained from Jackson laboratories were

bred with LysMcre to produce B6.129(Cg)-Gt(ROSA)26Sor$^{tm4(ACTB-tdTomato,-EGFP)Luo}$/J/LysMcre (ROSA-LysM) mice. The ROSA$^{mT/mG}$ allele is a Cre reporter that expresses cell membrane targeted two-color fluorescence. In these mice prior to Cre recombinase exposure, most cells/tissues express red fluorescence. After the exposure to Cre recombinase the target cells and future cell lineages derived from these cells express membrane-localized green fluorescence protein. Therefore, when bred with LysMcre animals all cells of myeloid origin express GFP. The MFG-E8-wildtype (MFG-E8$^{+/+}$) and MFG-E8-knockout (MFG-E8$^{-/-}$) mice were kindly provided by Dr. S. Nagata (Osaka University Medical School). In brief, the ES clones harboring the MFG-E8–deficient allele were injected to the host embryos to produce chimeric mice. The resultant chimeric mice were bred with C57BL/6 mice to produce MFG-E8$^{+/-}$ mice. The MFG-E8$^{+/-}$ mice were backcrossed with C57bl/6 for 12 generations which were in turn were bred to generate the MFG-E8$^{+/+}$ and MFG-E8$^{-/-}$ littermates (19). A splinted full thickness excisional wound model was employed as described previously (7, 20-21). Briefly, the dorsal side of the mice was naired and cleaned using betadine under anaesthesia. Two 6-mm diameter full thickness (skin and panniculus carnosus) excisional wounds were made on the dorsal skin with a 6-mm disposable biopsy punch (22-23). A donut-shaped splint with an 8-mm inner diameter was made from an 0.5-mm thick silicone sheet (Grace Bio-Laboratories, Bend, OR) and placed on the wound using an immediate-bonding adhesive, followed by interrupted 5-0 nylon sutures (Ethicon, Somerville, NJ), such that the wound was centered within the splint (7, 22). The wound was covered with semi-occlusive dressing (Tegaderm™; 3M, St. Paul, MN). For effective topical recombinant mouse MFG-E8 (R&D Systems, Minneapolis, MN) application, the protein solution was injected under the Tegaderm™. This approach has effectively delivered recombinant protein delivery to mice excisional wounds (23). Wound imaging was performed at specified times using a digital camera and the wound area was determined using Image J software (20). The animals were euthanized at specific times and wound tissues were harvested for molecular and histological analysis. All the animal studies were performed in accordance with protocols approved by the Laboratory Animal Care and Use Committee of the Ohio State University.

Isolation of murine wound mϕ and BMDM

For wound mϕ (ωmϕ), circular (8 mm) sterile PVA sponges were implanted subcutaneously on the backs of 8 to 12 week-old mice (7). Sponge-infiltrated wound mϕ were isolated as previously described (7, 23). Bone marrow-derived monocytes (BMDM) were isolated as previously described (23). Briefly, the femurs of mice (8-12 weeks old) were flushed using RPMI 1640 followed by positive selection of the flushed cells using magnetic beads conjugated CD11b Ab. The isolated d0 CD11b positive BMDMs were used for experiments.

“Hunt–Schilling” wire mesh cylinder for wound fluid collection

Wire mesh cylinders (stainless steel; 2.5cm length and 0.8cm diameter) were implanted and wound fluid was harvested as described previously (24). Briefly, following anesthesia, midline incision (1 cm or smaller) was made on shaved skin with a scalpel. Two small subcutaneous pockets were created by blunt dissection on either sides of the midline in which wire mesh stainless steel cylinders were implanted. The incisions were closed using sutures. Wound fluid was collected at d3 post-implantation.

Bone Marrow chimera

Bone marrow (BM) chimera was performed as previously described (25). For establishing chimerism, BM recipient male mice (6-8 weeks old) were injected intraperitoneally with busulfan in a 1:1 solution of DMSO and deionized water (30 mg/kg/100μl) once daily for 2 consecutive days resulting in partial ablation of the bone marrow. Whole body irradiation, resulting in myeloablation for bone marrow transplantation, is known to result in systemic toxicities (26). Moreover, irradiation is also expected to result in late side effects such as inflammation in skin (27). To circumvent these issues, we chose to use a myelosupressive approach for partial bone marrow ablation using busulfan which is an emergent solution that is being widely embraced depending on the specific questions addressed in a given study (25, 28-29). In our case, it was important to avoid the above-mentioned confounding factors that come with whole body irradiation. Donor BM-derived cells isolated from the femur were injected to recipient mice by tail vein injection (100μl) 48 h after the second dose of busulfan. Donor BM-derived cells were obtained from C57BL/6-Tg (CAG-EGFP), MFG-$E8^{+/+}$ or MFG-$E8^{-/-}$ mice. Following bone marrow transfer, mice were left undisturbed for 4 weeks to allow engraftment which was ascertained by determining the presence of GFP cells in the BM and the blood.

Apoptotic Cell Clearance Assay

Apoptotic cell clearance assay (efferocytosis) was performed as previously described (7). Briefly, wound mϕ were co-cultured in 8-well chambered slides with apoptotic (5 μM dexamethasone treated for 12 h; yield >90% PS positive thymocytes) thymocytes (labeled with pHrodo™ succinimidyl ester; Invitrogen) in 1:10 mϕ:thymocyte ratio. Efferocytosis studies were performed using cultured mϕ *ex vivo* for 1 h at 37°C followed by extensive washes to remove non-engulfed cells. Cells were then fixed with 4% paraformaldehyde and stained using F4/80-FITC followed by imaging using a fluorescence microscope. Efferocytosis index was calculated as the total number of engulfed apoptotic cells per mϕ present in the field of view (7, 30-31).

GeneChip® Probe Array Analyses

RNA extraction, target labeling, GeneChip® and data analysis were performed as described previously (21, 32). Briefly, *in vitro* transcription (IVT) reaction was performed using GeneChip® IVT Labeling Kit (Affymetrix, Santa Clara, CA) to generate biotinylated cRNA from RNA samples. The samples were hybridized to Affymetrix Mouse Genome U133 Plus 2.0 Array. The arrays were washed, stained with streptavidin-phycoerythrin and scanned with the GeneArray scanner (Affymetrix) in our own facilities as described earlier (21, 32) GCOS (Gene Chip Operating Software, Affymetrix) was employed for data acquisition and image processing. The expression data have been submitted to the Gene Expression Omnibus (GEO; http://www.ncbi.nlm.nih.gov/geo) with the series accession number GSE73229. Raw data were analyzed using Genespring GX (Agilent, Santa Clara CA). Additional processing of data was performed using dChip software (Harvard University) (21, 32).

Immunohistochemistry (IHC)

Immunostaining of CD31 and MFG-E8 was performed on cryosections of wound tissue samples using specific antibodies as described previously (33) (22). Briefly, 10 μm thick cryosectioned tissues were fixed with cold acetone, blocked with 10% normal goat serum and incubated with specific antibodies against CD31 (BD Pharmingen; 5550546, 1:400) and MFG-E8 (MBL International; 1:100) overnight at 4°C. Signal was visualized by subsequent incubation with fluorescence-tagged secondary antibodies (Alexa 568-tagged α-rat, 1:200; Alexa 405-tagged α-hamster, 1:200) followed by counterstaining with DAPI. Images were captured by microscope and quantification of fluorescent intensity of image was performed using AxioVision Rel 4.6 (Carl Zeiss Microimaging) software. Co-localization of immunostains was performed using FV10-ASW software from Olympus.

ELISA

Levels of MFG-E8, TNF-α and IL-10 (R & D Systems, Minneapolis, MN) were measured using commercially available ELISA kits (23, 31). The serum levels of MFG-E8 in murine wound fluid was measured using ELISA as described (34). In brief, phosphatidylserine solution in methanol was coated onto 96-well plates followed by blocking the wells with bovine serum albumin (BSA; 10 mg/ml). The serum was added to the wells and incubated at room temperature for 2h followed by washing with PBS containing 0.05% Tween 20. The MFG-E8 bound to the wells was detected using anti-MFG-E8 (mouse) mAb (MBL Int. Corp.; Clone 18A2-G10) and HRP linked anti-hamster secondary antibody. The levels of MFG-E8 in wound fluid were normalized against albumin concentration in the fluid (23). Albumin levels were determined by ELISA (AssayPro, St. Charles, MO) (23).

RNA extraction, reverse transcription and quantitative RT-PCR (qRT-PCR)

mirVana RNA isolation kit (Ambion, Austin, TX) was used according to the manufacturer's instructions to extract total RNA as previously described (18). Quantification of mRNA was done by real-time or quantitative (Q)PCR assay using double-stranded DNA binding dye SYBR Green-I, as described previously(21, 32, 35).

Matrigel® Assay

In vitro angiogenesis assay were assessed by tube formation ability on Matrigel® culture as described previously (33) (22, 36). Murine dermal endothelial cells (Cell Biologics, Inc. IL) were seeded on Matrigel® (Cultrex® Basement membrane extract reduced growth factor; R&D Systems, Minneapolis, MN) pre-coated four-well plates at a density of 8×10^4 cells/well. The angiogenic ability of 24h cell supernatants (conditioned media) from day 7 wound mϕ (treated with/without Recombinant MFG-E8 and recombinant VEGF; R&D Systems, Minneapolis, MN) of MFG-$E8^{+/+}$ WT and MFG-$E8^{-/-}$ mice was assessed 8 h after plating on Matrigel®, followed by staining with 3 μM calcein-AM (Invitrogen) for 20–30 min at 37 °C and 5% CO_2 as previously described (37). The tube length was measured using the software AxioVision Rel 4.6 (Zeiss) (20, 22).

Western blot

Western blot was performed using primary Ab against MFG-E8 (MBL International), phospho-MerTK (FabGennix, 1:750) and active Caspase 3 (Cell Signaling) as described previously(24, 31, 38). Signal was visualized using corresponding HRP-conjugated secondary antibody (Amersham, 1:3,000) and ECL Plus™ Western Blotting Detection Reagents (Amersham). β-actin (Sigma-Aldrich, 1:5000) served as loading control.

Wound vascularity and blood flow

Wound vascularity—Prior to sacrifice of mice, space-filling carboxylate-modified fluorescent microspheres (FluoSpheres, 0.2 μm, 1012 particles/ml) were injected into the left ventricle of the beating heart as previously described (24, 39).

Laser Speckle—Dermal blood flow was analyzed by laser speckle imager as described previously (40). The mean blood flow was measured in excisional wounds using PeriCam PSI System within a 100 mm^2 surface area (resolution 0.54 × 0.54 mm, working distance 10-20 cm).

Immunoprecipitation

Immunoprecipitation (IP) of MFG-E8 was done as previously described (41-42). Wound-edge tissue lysates (100μg) of diabetic animals were incubated with 5 μg of MFG-E8 mAb (clone 2422) overnight in a rotisserie shaker at 4°C. Protein A-agarose beads (Invitrogen) were prewashed with lysis buffer (150 mM KCl, 25 mM Tris-HCl, 5 mM EDTA, 0.5% IgePal, 1 mM PMSF, protease inhibitor) and incubated with the lysate-antibody mix for 3h at 4°C to immunoprecipitate MFG-E8. The beads were then washed three times with ice-cold lysis buffer and the immunoprecipitated complexes were washed four times with lysis buffer. For Western blot, the IP samples were subjected to SDS/PAGE after reduction with 1M DTT as previously described (37, 41) and probed with anti-AGE antibody (1: 1000 dilution, Abcam). The membrane was stripped and reprobed with anti-MFG-E8 antibody (Clone 18A2-G10).

MFG-E8 glycation and Surface-plasmon resonance analysis (Biacore)

For glycation of MFG-E8, 50μg of recombinant mouse MFG-E8 (R&D Systems) was treated with 10mM methylglyoxal (MGO, Sigma) at 37°C. To obtain dose dependent glycation, the reaction with MGO was performed for specific durations (0, 3h and 48h). The glycation of MFG-E8 was determined using Pierce™ Glycoprotein Carbohydrate Estimation kit (Pierce). The binding affinity of MFG-E8 and glyacted MFG-E8 to phosphatidylserine was analysed on Sensor chip L1 (GE Heathcare life Sciences) using Biacore T100 (43-44).

Data collection and statistical analyses

For *in vitro* experiments, data are reported as mean ± SD of 3–6 experiments as indicated in respective figure legends. For animal studies, data are reported as mean ± SD of at least 3-8 animals as indicated. For human wound fluid studies, data from human subjects (n = 10) have been presented (Table 1). Student's t test (two-tailed) was used to determine significant

differences. Comparisons among multiple groups were tested using analysis of variance (ANOVA). $p<0.05$ was considered statistically significant.

Results

MFG-E8 deficiency impairs wound closure and wound re-epithelialization

MFG-E8$^{-/-}$ and age-matched MFG-E8$^{+/+}$ mice were used to test the significance of MFG-E8 in wound healing. MFG-E8$^{-/-}$ mice exhibited significantly delayed wound closure kinetics as compared to the wild type age matched littermates. By d10, when ~90% of the wounds of the wild type animals were fully closed, the wounds of null mice were still 60% open **(Fig 1 A-B)**. Wound re-epithelialization was significantly impaired on d5-10 post-wounding in null mice as compared to the wild type animals **(Fig 1 C-D)**. Loss of MFG-E8 protein in the skin of null mice was confirmed by Western blot **(Fig 1E)**.

Expressed by wound-site macrophages, MFG-E8 supports efferocytosis and resolves wound inflammation

Wound-edge tissues were collected on d3, 5, 7, and 10 post-wounding to study the abundance of MFG-E8. A significant increase in wound-edge MFG-E8 protein was noted on d3 & 5 post-wounding **(Fig 2A)**. To determine whether MFG-E8 is induced in wound mϕ, MFG-E8 expression in wound mϕ was compared with monocytes derived from bone marrow (BMDM). Although MFG-E8 was almost undetectable in BMDM, MFG-E8 in d3 wound mϕ was abundant **(Fig 2B)**. MFG-E8-L form and not the -S form has been shown to serve as a linker between phagocytic cells and apoptotic cells (15). The -L form, is produced by macrophages (15) and was found to be predominantly expressed in the skin using a MFG-E8 antibody raised in hamster (MBL Inc., Clone 18A2-G10) (**Fig 2A**).

The cells/tissue of B6.129(Cg)-Gt(ROSA)26Sor$^{tm4(ACTB-tdTomato,-EGFP)Luo}$/J/LysMcre (ROSA-LysM) mice widely express cell membrane-localized red fluorescence. However, because of LysM-driven cre-recombinase, only the cells of myeloid origin express membrane-localized green fluorescence. Expectedly, the wound mϕ (GFP^{+}, green) abundance at the wound-site peaked on d3 and 5 post-wounding (**Fig 2C**). Using these ROSA-LysM mice, we investigated the significance of mϕ as a source of MFG-E8 in wounds. The increase of wound-site MFG-E8 levels was co-incident with the kinetics of mϕ recruitment to the site **(Fig 2C, S1)**. Immunohistochemical staining of MFG-E8 in d3 wound-edge tissue of ROSA-LysM mice showed that 65% of wound-site MFG-E8 signal was co-localized with wound **(Fig 2D)**. Taken together, these data reveal that during the inflammatory phase (d3-5 post wounding), wound mϕ are a major source of MFG-E8 at the wound-site **(Fig 2B-D).**

MFG-E8 serves as a bridging molecule between apoptotic cells and phagocytes enabling efferocytosis (15). Wound mϕ from MFG-E8$^{-/-}$ mice exhibited significantly compromised efferocytosis activity compared to those from the wild-type animals **(Fig 3A-B)**. Successful efferocytosis is known to suppress pro-inflammatory and upregulate anti-inflammatory genes (30, 45). iNOS and Arginase are classical markers for M1 and M2 macrophages, respectively (46). Consistently, non-efferocytosing mφ from MFG-E8$^{-/-}$ mice showed a pro-

inflammatory M1 phenotype featuring high pro-inflammatory iNOS and low anti-inflammatory Arginase **(Fig S2)**.

Mer tyrosine kinase (MerTK), a member of the Axl/Mer/Tyro3 receptor tyrosine kinase (RTK) family, is required for efferocytosis by mϕ (47). The phosphorylation of MerTK was determined as an additional evidence of impaired efferocytosis in MFG-E8$^{-/-}$. Post-efferocytotic wound mϕ from MFG-E8$^{-/-}$ mice exhibited lower MerTK phosphorylation (**Fig 3C)**. Efferocytosis is known to cause MerTK phosphorylation (48-50). This is consistent with our observation that impaired efferocytosis **(Fig 3A-B)** in MFG-E8$^{-/-}$ mice blunted MerTK phosphorylation post-efferocytosis. Apoptotic cell burden at the wound-edge tissue was measured by immunoblotting active caspase 3. The d7 wound-edge tissue from MFG-E8$^{-/-}$ exhibited significantly higher active caspase-3 levels as compared to wild-type wound tissues indicating higher apoptotic cell burden **(Fig 3D)**.

Our laboratory has reported that increasing apoptotic cell burden at wound site results in prolonged inflammatory response (7). Consistently, wound-edge of MFG-E8$^{-/-}$ that were burdened with apoptotic cells, displayed a pro-inflammatory phenotype as exemplified by augmented levels of pro-inflammatory TNF-α **(Fig 3E)** and decreased levels of anti-inflammatory IL-10 **(Fig 3F)**.

Impaired wound angiogenesis in MFG-E8$^{-/-}$ mice

Timely resolution of wound inflammation is a prerequisite for the onset of wound angiogenesis (51-52). To elucidate the molecular mechanisms by which MFG-E8 supports wound healing, unbiased transcriptome profiling of wound-edge tissue (d5 post wounding) from MFG-E8$^{-/-}$ and control MFG-E8$^{+/+}$ mice was performed. Pathway analysis identified a distinct cluster of pro-angiogenic genes that were potently down regulated in the wound-edge of MFG-E8$^{-/-}$ animals **(Fig 4A-B)**. This data was further validated using qRT-PCR **(Fig 4C)**. Findings of transcriptome analysis were extended to examine whether indeed the wounds of MFG-E8$^{-/-}$ mice display impaired angiogenesis. Decreased abundance of wound-edge CD31+ endothelial cells was noted in the MFG-E8$^{-/-}$ mice **(Fig 4D, S3).** Wound vascularization was further monitored using fluorescent microspheres (0.2μm; fluoSpheres carboxylate-modified microspheres, green fluorescent; Molecular Probes) that were injected into the left ventricle (53) **(Fig 4E, S3).** A marked decrease in the number of green microspheres at the wound–site of MFG-E8$^{-/-}$ mice demonstrated compromised wound angiogenesis. Finally, the functional analysis of blood flow at the wound site performed using laser speckle perfusion imaging demonstrated a marked decrease in blood flow in MFG-E8$^{-/-}$ mice **(Fig 4F)**. These data collectively establish that at the wound-site MFG-E8 plays a critical role in supporting wound angiogenesis.

Wound macrophage derived MFG-E8 is angiogenic

To test the angiogenic potential of mϕ-derived MFG-E8, Matrigel® tube formation was performed using conditioned media (CM) from d7 wound mϕ of MFG-E8$^{-/-}$ and MFG-E8$^{+/+}$ mice. Tube formation of murine dermal endothelial cells was significantly better when incubated with CM from MFG-E8$^{+/+}$ mϕ compared to that in response to CM from MFG-E8$^{-/-}$ mϕ. Impairment of such tube formation in response to CM from MFG-E8$^{-/-}$ mϕ was

partially rescued by replenishing the CM with rMFG-E8. Adding both rMFG-E8 and rVEGF to the CM fully restored Matrigel® angiogenic response **(Fig 5A-B)**. Furthermore, the expression of major angiogenic genes was significantly downregulated in the wound mϕ of MFG-E8$^{-/-}$ mice **(Fig 5C-E)**. Thus, in wound mϕ, MFG-E8 is angiogenic.

To further test the significance of mϕ-derived MFG-E8 on wound angiogenesis and healing, bone marrow transplantation (BMT) was performed involving ablation of the bone marrow by busulphan injection followed by reconstitution using the donor bone marrow **(Fig S4)**. Transplantation of MFG-E8$^{-/-}$ bone marrow to MFG-E8$^{+/+}$ mice resulted in impaired wound closure **(Fig 6A-B)** and compromised wound vascularization **(Fig 6C-D)** compared to the MFG-E8$^{+/+}$ mice receiving wild-type bone marrow. On the other hand, MFG-E8$^{-/-}$ mice that received wild-type bone marrow showed improved wound closure **(Fig 6E-F)** and improved wound vascularization **(Fig 6G-H).** This line of evidence firmly establishes a significant angiogenic role wound mϕ-derived MFG-E8.

Lower MFG-E8 levels in the diabetic wound environment

MFG-E8 protein levels were determined in wound fluids obtained from patients with chronic wounds. The MFG-E8 level was significantly lower in the wound fluid from chronic wound patients with clinically diagnosed diabetes as compared to the fluids obtained from chronic wound patients without diabetes **(Fig 7A)**. Patient demographic is listed in **Table 1**. Consistent data were obtained in the wound fluids from diabetic mice (Lepr^{db}, db/db) as compared to age-matched non-diabetic controls (heterozygous, Lepr$^{db/+,}$ m+/db) **(Fig 7B)**. It is known that under diabetic conditions, hyperglycemia may cause non-enzymatic glycation of free amino groups of proteins that then leads to the structural and functional changes in these proteins. Such changes may mask immunodetection of MFG-E8, rich in RGD and P/T rich domains.

To determine if MFG-E8 is glycated in diabetic wounds, immunoprecipitation (IP) of MFG-E8 from diabetic wounds followed by cross blotting (IB) with anti-AGE antibody was performed. The data indicates that MFG-E8 in diabetic ulcers gets glycated **(Fig 7C)**. We tested if the binding affinity of MFG-E8 to phosphatidylserine (PS) is compromised following glycation of MFG-E8. Such binding affinity was tested using surface plasmon resonance (Biacore) with phosphotidylserine (PS) or phosphatidylcholine (as a reference) liposomes immobilized on the sensor chip and glycated MFG-E8 or native MFG-E8 as soluble analytes. MFG-E8 exhibited preferential binding with PC:PS (50:50 mol/mol) as compared to PC:PS (100:0 mol/mol). Glycated MFG-E8 displayed weak binding affinity to PS as compared to the binding of sham with PS **(Fig 7D-F)**. To obtain dose dependent glycation, the reaction with MGO was performed for specific durations (0, 3 and 48h). Such incubation resulted in significant differences in glycation of MFG-E8 at 3h and 48h **(Fig 7H)**. The dose dependent glycation of MFG-E8 resulted in dose dependent inactivation of MFG-E8 towards binding to PS as measured using Biacore **(Fig 7G)**. Thus, MFG-E8 is subject to glycemic modification resulting in loss of PS binding activity which in turn blunts efferocytosis.

MFG-E8 treatment improves efferocytosis, angiogenesis and healing in diabetic wounds

The treatment of isolated diabetic wound mϕ with MFG-E8 improved efferocytosis activity **(Fig. 8A)**. Topical treatment of diabetic wounds with rMFG-E8 (1μg each wound daily once) favored resolution of inflammation by lowering TNF-α levels and increasing anti-inflammatory IL-10 levels at the wound-edge tissue (**Fig 8B**). Resolution of inflammation is known to favor the wound angiogenesis cascade. Consistently, topical treatment of diabetic wounds with rMFG-E8 markedly improved wound angiogenesis **(Fig. 8C)**. These favorable effects of topical rMFG-E8 were eventually recorded as faster wound closure **(Fig 8D-E).**

Discussion

MFG-E8 is a peripheral glycoprotein which acts as a bridging molecule between the mϕ and apoptotic cells thus executing a pivotal role in the scavenging of apoptotic cells from affected tissues (15). Expressed and secreted by activated mϕ and dendritic cells, MFG-E8 is versatile, and displays a wide array of functions in cell physiology (15, 54). The therapeutic potential of this multi-domain protein has been recognized in a multitude of diseased conditions such as cancers, sepsis and ischemia-reperfusion injury of the heart and DSS-induced colitis (54-56) MFG-E8 has anti-inflammatory properties primarily executed by its effects on mϕ cell biology (57-58). Non-resolving inflammation is a key factor that underlies chronic wounds such as diabetic ulcers (2). The significance of MFG-E8 in managing wound inflammation is thus of extraordinary interest. The current study recognizes wound mϕ MFG-E8 function as being critical in resolving wound inflammation. Importantly, it upholds an extraordinary significance of MFG-E8 in effectively managing diabetic wound complications.

Wound-site mϕ are key drivers of the healing process (5, 8-9, 59). The site of injury is laden with dead cells. Timely debridement of apoptotic cells by wound-site mϕ paves the way to the resolution of inflammation (10-13). Under conditions of diabetic complications, such efferocytosis is compromised resulting in increased apoptotic cell burden at the wound-site. Inability of wound-site mϕ to execute efferocytosis results in a persisting pro-inflammatory *milieu* which complicates healing outcomes (7). Functionally, MFG-E8 enables efferocytosis by binding to phosphatidylserine (PS) on apoptotic cell surface and tethering them to mϕ via integrin receptors. However the origin of MFG-E8 is contentious and dependent on the context. In tumors, pericytes represent a major source of the secreted MFG-E8 (60). Although direct evidence was limited, inspired by the tumor findings it was speculated that pericytes are the primary source of MFG-E8 at the wound-site (17). The present study is the first to establish mϕ as the primary contributor of MFG-E8 in the inflammatory phase of cutaneous wound healing.

Cutaneous wounds of loose-skinned animals such as mice, unlike humans, primarily close by contraction. To study wound closure by granulation and re-epithelialization, as is relevant to humans, it is therefore required that cutaneous wounds be stented (61). Marginal compromise in wound closure as reported in non-stented MFG-E8$^{-/-}$ mice may be attributed to the heavy influence of wound contraction, as opposed to healing, under such experimental conditions (17). Results reported from stented wounds in MFG-E8$^{-/-}$ mice in the current study demonstrate remarkable impairment in wound closure recognizing MFG-E8 as a

significant player in the overall healing process. Significance of such observation was further heightened by rescue experiments involving MFG-E8$^{-/-}$ mice that were subjected to wild-type bone marrow transplantation. Also, transplantation of MFG-E8$^{-/-}$ bone marrow to MFG-E8$^{+/+}$ mice compromised wound healing. Thus, this work provides definitive evidence establishing MFG-E8 as a critical contributor to the wound healing process.

Mϕ are highly plastic and respond to environmental cues by adapting to classically activated (M1) proinflammatory or alternatively activated (M2) anti-inflammatory, pro-angiogenic phenotype (62-63). Efferocytosis serves as a cue for mϕ switching to an anti-inflammatory and pro-angiogenic (M2) phenotype (7, 10-11, 31, 64-65). MFG-E8 has profound influence in promoting VEGF-induced angiogenesis (16-17). Given that tissue mϕ have been directly implicated in angiogenesis (66-67), the question whether mϕ-dependent mechanisms are involved in executing the angiogenic functions of MFG-E8 remains open. The current work demonstrates that in cutaneous wounds of MFG-E8$^{-/-}$ mice, featuring persistent inflammation, wound angiogenesis is markedly compromised. Rescue experiments involving bone marrow transplantation add clarity to this important observation. In light of a central role of MFG-E8 in driving efferocytosis and thereby switching wound-site mϕ toward an anti-inflammatory and pro-angiogenic form (M2), it is conceivable that the pro-vascularization effects of MFG-E8 in the wound *milieu* may be dependent on its effects supporting efferocytosis and downstream mϕ polarization. This contention was further substantiated by the observation that conditioned media from wound mϕ from MFG-E8$^{+/+}$ mice displayed significantly improved angiogenic properties. Limited wound perfusion in a setting of persistent inflammation is commonly noted in diabetic ulcers. Whether limited MFG-E8 function is a causative factor complicating diabetic wound healing is therefore a reasonable question.

Previous work by our laboratory has recognized that an elevated apoptotic cell burden at wound-site exaggerates sustained inflammation at the wound-site (7). Furthermore, impaired efferocytosis by wound mϕ, increased apoptotic cell burden and persistent inflammatory response is a hallmark of diabetic wounds (7, 10-11). Results of the present work uphold deficiencies in MFG-E8 functioning as a key factor explaining impaired efferocytosis and resulting in persistent inflammation in diabetic wounds. In diabetes, hyperglycemia is known to cause non-enzymatic glycation of free amino groups of proteins which then leads to the structural and functional changes in these proteins resulting in changes in functionality (68). The irreversible formation of advanced glycation end products (AGEs) is one example that is known to drive numerous pathophysiological mechanisms relevant to diabetic complications (69). In MFG-E8, unique structural characteristics such as the presence of RGD and P/T rich domains make it susceptible to glycation. Indeed, methylglyoxal (MGO) a precursor molecule for AGE, is present at high levels in diabetic plasma (70). MGO is a potent arginine-directed glycating agent that forms hydroimidazolone derivative Nδ-(5-hydro-5-methyl-4-imidazolon-2-yl)-ornithine (MG-H1) residue with arginine (71). MG-H1, an AGE, is a product of glycation abundant in diabetes (71). This work study provides maiden evidence demonstrating that MFG-E8 is not only sensitive to glycation in diabetic wounds also as predicted by its structure, but that glycation has a major impact on MFG-E8 function. That glycated MFG-E8 suffers from loss of binding activity towards PS resulting in impaired efferocytosis by diabetic wound mϕ is of substantial significance addressing

chronic inflammation and poor perfusion commonly noted in diabetic ulcers. From a therapeutic standpoint, this work presents topical application of rMFG-E8 as a productive approach to circumvent blockade in the functioning of glycated endogenous MFG-E8. From a mechanistic standpoint, this finding highlights the importance of rescuing efferocytosis in diabetic wounds.

Wound healing biology has always been viewed as a continuum of multiple processes that act in a synergistic and coordinated manner to achieve closure of the defect. Although processes such as inflammation, angiogenesis and re-epithelialization are often studied as separated pieces for the sake of gaining traction in a somewhat simplified scenario there is little doubt that these processes engage in sophisticated cross-talk and that such interplay is critical to achieving successful healing. This work recognizes mϕ-derived MFG-E8 as an influential commander of such cross-talk positioned at the seams of inflammation, angiogenesis and re-epithelialization. Effective dead cell clearance at the wound-site, enabled by MFG-E8, advances mϕ towards resolution of inflammation. Such resolution of inflammation in turn advances wound angiogenesis. As it relates to angiogenesis, MFG-E8 is capable of bolstering signaling of VEGF helping perfuse the wound tissue. Resolution of inflammation together with effective wound vascularization supports re-epithelialization and wound closure. Above and beyond positioning MFG-E8 as master of a key hub in wound healing, this work recognizes that MFG-E8 may become defunct under conditions of hyperglycemia and exposure to AGE. Indeed, loss of MFG-E8 function impairs diabetic wound healing. From a therapeutic standpoint, it is of extraordinary interest that topical application of rMFG-E8 is effective in restoring MFG-E8 function in diabetic wounds. Topical rMFG-E8 induced resolution of wound inflammation, improvements in angiogenesis and acceleration of closure upholding the potential of MFG-E8 directed therapeutics in diabetic wound care.

Supplementary Material

Refer to Web version on PubMed Central for supplementary material.

Acknowledgments

Wound healing research in the authors' laboratory is funded by NIDDK R01 DK076566 & NINR NR015676 to SR; NIGMS R01 GM069589, GM 077185 & NINR NR013898 & NR015676 to CKS.

Abbreviations used

VEGF	Vascular endothelial growth factor
BMDM	Bone marrow-derived monocytes
iNOS	inducible Nitric Oxide Synthase
TNC	Tenascin C
THBS1	Thrombospondin 1
TNFAIP2	Tumor Necrosis Factor, Alpha-Induced Protein 2

ZEB2 Zinc Finger E-Box Binding Homeobox 2

References

1. Sen CK, Gordillo GM, Roy S, Kirsner R, Lambert L, Hunt TK, Gottrup F, Gurtner GC, Longaker MT. Human skin wounds: a major and snowballing threat to public health and the economy. Wound Repair Regen. 2009; 17:763–771. [PubMed: 19903300]
2. Falanga V. Wound healing and its impairment in the diabetic foot. Lancet. 2005; 366:1736–1743. [PubMed: 16291068]
3. Pierce GF. Inflammation in nonhealing diabetic wounds: the space-time continuum does matter. Am J Pathol. 2001; 159:399–403. [PubMed: 11485896]
4. Brem H, Tomic-Canic M. Cellular and molecular basis of wound healing in diabetes.[comment]. Journal of Clinical Investigation. 2007; 117:1219–1222. [PubMed: 17476353]
5. Eming SA, Krieg T, Davidson JM. Inflammation in wound repair: molecular and cellular mechanisms. J Invest Dermatol. 2007; 127:514–525. [PubMed: 17299434]
6. Serhan CN. Systems approach to inflammation resolution: identification of novel anti-inflammatory and pro-resolving mediators. J Thromb Haemost. 2009; 7(Suppl 1):44–48. [PubMed: 19630766]
7. Khanna S, Biswas S, Shang Y, Collard E, Azad A, Kauh C, Bhasker V, Gordillo GM, Sen CK, Roy S. Macrophage dysfunction impairs resolution of inflammation in the wounds of diabetic mice. PLoS One. 2010; 5:e9539. [PubMed: 20209061]
8. Goren I, Allmann N, Yogev N, Schurmann C, Linke A, Holdener M, Waisman A, Pfeilschifter J, Frank S. A transgenic mouse model of inducible macrophage depletion: effects of diphtheria toxin-driven lysozyme M-specific cell lineage ablation on wound inflammatory, angiogenic, and contractive processes. Am J Pathol. 2009; 175:132–147. [PubMed: 19528348]
9. Mirza R, DiPietro LA, Koh TJ. Selective and specific macrophage ablation is detrimental to wound healing in mice. Am J Pathol. 2009; 175:2454–2462. [PubMed: 19850888]
10. Roy, S., editor. Resolution of Inflammation in Wound Healing:Significance of Dead Cell Clearance. Mary Ann Liebert, Inc.; New York: 2010.
11. Das, A.; Roy, S. Resolution of Inflammation. In: Sashwati Roy, DB.; Raychaudhuri, Siba P., editors. Chronic Inflammation: Molecular Pathophysiology, Nutritional and Therapeutic Interventions. CRC Press; 2013. p. 119-128.
12. Serhan CN, Brain SD, Buckley CD, Gilroy DW, Haslett C, O'Neill LA, Perretti M, Rossi AG, Wallace JL. Resolution of inflammation: state of the art, definitions and terms. FASEB J. 2007; 21:325–332. [PubMed: 17267386]
13. Maskrey BH, Megson IL, Whitfield PD, Rossi AG. Mechanisms of resolution of inflammation: a focus on cardiovascular disease. Arterioscler Thromb Vasc Biol. 2011; 31:1001–1006. [PubMed: 21508346]
14. Yamazaki M, Maruyama S, Abe T, Essa A, Babkair H, Cheng J, Saku T. MFG-E8 expression for progression of oral squamous cell carcinoma and for self-clearance of apoptotic cells. Lab Invest. 2014; 94:1260–1272. [PubMed: 25264705]
15. Hanayama R, Tanaka M, Miwa K, Shinohara A, Iwamatsu A, Nagata S. Identification of a factor that links apoptotic cells to phagocytes. Nature. 2002; 417:182–187. [PubMed: 12000961]
16. Silvestre JS, Thery C, Hamard G, Boddaert J, Aguilar B, Delcayre A, Houbron C, Tamarat R, Blanc-Brude O, Heeneman S, Clergue M, Duriez M, Merval R, Levy B, Tedgui A, Amigorena S, Mallat Z. Lactadherin promotes VEGF-dependent neovascularization. Nat Med. 2005; 11:499–506. [PubMed: 15834428]
17. Uchiyama A, Yamada K, Ogino S, Yokoyama Y, Takeuchi Y, Udey MC, Ishikawa O, Motegi S. MFG-E8 regulates angiogenesis in cutaneous wound healing. Am J Pathol. 2014; 184:1981–1990. [PubMed: 24838098]
18. Roy S, Dickerson R, Khanna S, Collard E, Gnyawali U, Gordillo GM, Sen CK. Particulate beta-glucan induces TNF-alpha production in wound macrophages via a redox-sensitive NF-kappabeta-dependent pathway. Wound Repair Regen. 2011; 19:411–419. [PubMed: 21518092]

19. Hanayama R, Tanaka M, Miyasaka K, Aozasa K, Koike M, Uchiyama Y, Nagata S. Autoimmune disease and impaired uptake of apoptotic cells in MFG-E8-deficient mice. Science. 2004; 304:1147–1150. [PubMed: 15155946]
20. Chan YC, Roy S, Huang Y, Khanna S, Sen CK. The microRNA miR-199a-5p down-regulation switches on wound angiogenesis by derepressing the v-ets erythroblastosis virus E26 oncogene homolog 1-matrix metalloproteinase-1 pathway. J Biol Chem. 2012; 287:41032–41043. [PubMed: 23060436]
21. Roy S, Khanna S, Rink C, Biswas S, Sen CK. Characterization of the acute temporal changes in excisional murine cutaneous wound inflammation by screening of the wound-edge transcriptome. Physiol Genomics. 2008; 34:162–184. [PubMed: 18460641]
22. Chan YC, Roy S, Khanna S, Sen CK. Downregulation of endothelial microRNA-200b supports cutaneous wound angiogenesis by desilencing GATA binding protein 2 and vascular endothelial growth factor receptor 2. Arterioscler Thromb Vasc Biol. 2012; 32:1372–1382. [PubMed: 22499991]
23. Ganesh K, Das A, Dickerson R, Khanna S, Parinandi NL, Gordillo GM, Sen CK, Roy S. Prostaglandin E(2) induces oncostatin M expression in human chronic wound macrophages through Axl receptor tyrosine kinase pathway. J Immunol. 2012; 189:2563–2573. [PubMed: 22844123]
24. Roy S, Khanna S, Nallu K, Hunt TK, Sen CK. Dermal wound healing is subject to redox control. Mol Ther. 2006; 13:211–220. [PubMed: 16126008]
25. Wohleb ES, Powell ND, Godbout JP, Sheridan JF. Stress-induced recruitment of bone marrow-derived monocytes to the brain promotes anxiety-like behavior. J Neurosci. 2013; 33:13820–13833. [PubMed: 23966702]
26. Peake K, Manning J, Lewis CA, Barr C, Rossi F, Krieger C. Busulfan as a myelosuppressive agent for generating stable high-level bone marrow chimerism in mice. J Vis Exp. 2015:e52553. [PubMed: 25867947]
27. Goertz O, Poettgen C, Akbari A, Kolbenschlag J, Langer S, Lehnhardt M, Stuschke M, von der Lohe L. New model for long-term investigations of cutaneous microcirculatory and inflammatory changes following irradiation. J Radiat Res. 2015; 56:456–461. [PubMed: 25691452]
28. Wohleb ES, McKim DB, Shea DT, Powell ND, Tarr AJ, Sheridan JF, Godbout JP. Re-establishment of anxiety in stress-sensitized mice is caused by monocyte trafficking from the spleen to the brain. Biol Psychiatry. 2014; 75:970–981. [PubMed: 24439304]
29. Lewis CA, Manning J, Barr C, Peake K, Humphries RK, Rossi F, Krieger C. Myelosuppressive conditioning using busulfan enables bone marrow cell accumulation in the spinal cord of a mouse model of amyotrophic lateral sclerosis. PLoS One. 2013; 8:e60661. [PubMed: 23593276]
30. Huynh ML, Fadok VA, Henson PM. Phosphatidylserine-dependent ingestion of apoptotic cells promotes TGF-beta1 secretion and the resolution of inflammation. J Clin Invest. 2002; 109:41–50. [PubMed: 11781349]
31. Das A, Ganesh K, Khanna S, Sen CK, Roy S. Engulfment of apoptotic cells by macrophages: a role of microRNA-21 in the resolution of wound inflammation. J Immunol. 2014; 192:1120–1129. [PubMed: 24391209]
32. Roy S, Patel D, Khanna S, Gordillo GM, Biswas S, Friedman A, Sen CK. Transcriptome-wide analysis of blood vessels laser captured from human skin and chronic wound-edge tissue. Proc Natl Acad Sci U S A. 2007; 104:14472–14477. [PubMed: 17728400]
33. Shilo S, Roy S, Khanna S, Sen CK. Evidence for the involvement of miRNA in redox regulated angiogenic response of human microvascular endothelial cells. Arterioscler Thromb Vasc Biol. 2008; 28:471–477. [PubMed: 18258815]
34. Yamaguchi H, Takagi J, Miyamae T, Yokota S, Fujimoto T, Nakamura S, Ohshima S, Naka T, Nagata S. Milk fat globule EGF factor 8 in the serum of human patients of systemic lupus erythematosus. J Leukoc Biol. 2008; 83:1300–1307. [PubMed: 18303131]
35. Roy S, Driggs J, Elgharably H, Biswas S, Findley M, Khanna S, Gnyawali U, Bergdall VK, Sen CK. Platelet-rich fibrin matrix improves wound angiogenesis via inducing endothelial cell proliferation. Wound Repair Regen. 2011; 19:753–766. [PubMed: 22092846]

36. Chan YC, Khanna S, Roy S, Sen CK. miR-200b targets Ets-1 and is down-regulated by hypoxia to induce angiogenic response of endothelial cells. The Journal of biological chemistry. 2011; 286:2047–2056. [PubMed: 21081489]
37. Gordillo GM, Biswas A, Khanna S, Pan X, Sinha M, Roy S, Sen CK. Dicer knockdown inhibits endothelial cell tumor growth via microRNA 21a-3p targeting of Nox-4. The Journal of biological chemistry. 2014; 289:9027–9038. [PubMed: 24497637]
38. Roy S, Khanna S, Rink T, Radtke J, Williams WT, Biswas S, Schnitt R, Strauch AR, Sen CK. P21waf1/cip1/sdi1 as a central regulator of inducible smooth muscle actin expression and differentiation of cardiac fibroblasts to myofibroblasts. Mol Biol Cell. 2007; 18:4837–4846. [PubMed: 17881730]
39. Jacobi J, Jang JJ, Sundram U, Dayoub H, Fajardo LF, Cooke JP. Nicotine accelerates angiogenesis and wound healing in genetically diabetic mice. Am J Pathol. 2002; 161:97–104. [PubMed: 12107094]
40. Elgharably H, Roy S, Khanna S, Abas M, Dasghatak P, Das A, Mohammed K, Sen CK. A modified collagen gel enhances healing outcome in a preclinical swine model of excisional wounds. Wound Repair Regen. 2013; 21:473–481. [PubMed: 23607796]
41. Roy S, Khanna S, Azad A, Schnitt R, He G, Weigert C, Ichijo H, Sen CK. Fra-2 mediates oxygen-sensitive induction of transforming growth factor beta in cardiac fibroblasts. Cardiovasc Res. 2010; 87:647–655. [PubMed: 20427335]
42. Park HA, Khanna S, Rink C, Gnyawali S, Roy S, Sen CK. Glutathione disulfide induces neural cell death via a 12-lipoxygenase pathway. Cell Death Differ. 2009; 16:1167–1179. [PubMed: 19373248]
43. He M, Kubo H, Morimoto K, Fujino N, Suzuki T, Takahasi T, Yamada M, Yamaya M, Maekawa T, Yamamoto Y, Yamamoto H. Receptor for advanced glycation end products binds to phosphatidylserine and assists in the clearance of apoptotic cells. EMBO reports. 2011; 12:358–364. [PubMed: 21399623]
44. Small H, Gardner I, Jones HM, Davis J, Rowland M. Measurement of binding of basic drugs to acidic phospholipids using surface plasmon resonance and incorporation of the data into mechanistic tissue composition equations to predict steady-state volume of distribution. Drug Metab Dispos. 2011; 39:1789–1793. [PubMed: 21764943]
45. Fadok VA, Bratton DL, Konowal A, Freed PW, Westcott JY, Henson PM. Macrophages that have ingested apoptotic cells in vitro inhibit proinflammatory cytokine production through autocrine/paracrine mechanisms involving TGF-beta, PGE2, and PAF. J Clin Invest. 1998; 101:890–898. [PubMed: 9466984]
46. Rath M, Muller I, Kropf P, Closs EI, Munder M. Metabolism via Arginase or Nitric Oxide Synthase: Two Competing Arginine Pathways in Macrophages. Front Immunol. 2014; 5:532. [PubMed: 25386178]
47. Cohen PL, Caricchio R, Abraham V, Camenisch TD, Jennette JC, Roubey RA, Earp HS, Matsushima G, Reap EA. Delayed apoptotic cell clearance and lupus-like autoimmunity in mice lacking the c-mer membrane tyrosine kinase. J Exp Med. 2002; 196:135–140. [PubMed: 12093878]
48. Seitz HM, Camenisch TD, Lemke G, Earp HS, Matsushima GK. Macrophages and dendritic cells use different Axl/Mertk/Tyro3 receptors in clearance of apoptotic cells. J Immunol. 2007; 178:5635–5642. [PubMed: 17442946]
49. Nishi C, Toda S, Segawa K, Nagata S. Tim4- and MerTK-mediated engulfment of apoptotic cells by mouse resident peritoneal macrophages. Mol Cell Biol. 2014; 34:1512–1520. [PubMed: 24515440]
50. Todt JC, Hu B, Curtis JL. The receptor tyrosine kinase MerTK activates phospholipase C gamma2 during recognition of apoptotic thymocytes by murine macrophages. J Leukoc Biol. 2004; 75:705–713. [PubMed: 14704368]
51. Elgharably H, Ganesh K, Dickerson J, Khanna S, Abas M, Ghatak PD, Dixit S, Bergdall V, Roy S, Sen CK. A modified collagen gel dressing promotes angiogenesis in a preclinical swine model of chronic ischemic wounds. Wound Repair Regen. 2014; 22:720–729. [PubMed: 25224310]

52. Weisser SB, McLarren KW, Kuroda E, Sly LM. Generation and characterization of murine alternatively activated macrophages. Methods Mol Biol. 2013; 946:225–239. [PubMed: 23179835]
53. Springer ML, Ip TK, Blau HM. Angiogenesis monitored by perfusion with a space-filling microbead suspension. Mol Ther. 2000; 1:82–87. [PubMed: 10933915]
54. Li BZ, Zhang HY, Pan HF, Ye DQ. Identification of MFG-E8 as a novel therapeutic target for diseases. Expert Opin Ther Targets. 2013; 17:1275–1285. [PubMed: 23972256]
55. Raymond A, Ensslin MA, Shur BD. SED1/MFG-E8: a bi-motif protein that orchestrates diverse cellular interactions. J Cell Biochem. 2009; 106:957–966. [PubMed: 19204935]
56. Otani A, Ishihara S, Aziz MM, Oshima N, Mishima Y, Moriyama I, Yuki T, Amano Y, Ansary MM, Kinoshita Y. Intrarectal administration of milk fat globule epidermal growth factor-8 protein ameliorates murine experimental colitis. Int J Mol Med. 2012; 29:349–356. [PubMed: 22200667]
57. Aziz M, Jacob A, Matsuda A, Wu R, Zhou M, Dong W, Yang WL, Wang P. Pre-treatment of recombinant mouse MFG-E8 downregulates LPS-induced TNF-alpha production in macrophages via STAT3-mediated SOCS3 activation. PLoS One. 2011; 6:e27685. [PubMed: 22114683]
58. Miksa M, Wu R, Dong W, Das P, Yang D, Wang P. Dendritic cell-derived exosomes containing milk fat globule epidermal growth factor-factor VIII attenuate proinflammatory responses in sepsis. Shock. 2006; 25:586–593. [PubMed: 16721266]
59. Leibovich SJ, Ross R. The role of the macrophage in wound repair. A study with hydrocortisone and antimacrophage serum. Am J Pathol. 1975; 78:71–100. [PubMed: 1109560]
60. Motegi S, Leitner WW, Lu M, Tada Y, Sardy M, Wu C, Chavakis T, Udey MC. Pericyte-derived MFG-E8 regulates pathologic angiogenesis. Arterioscler Thromb Vasc Biol. 2011; 31:2024–2034. [PubMed: 21737783]
61. Galiano RD, Michaels J. t. Dobryansky M, Levine JP, Gurtner GC. Quantitative and reproducible murine model of excisional wound healing. Wound Repair Regen. 2004; 12:485–492. [PubMed: 15260814]
62. Das A, Sinha M, Datta S, Abas M, Chaffee S, Sen CK, Roy S. Monocyte and Macrophage Plasticity in Tissue Repair and Regeneration. Am J Pathol. 2015; 185:2596–2606. [PubMed: 26118749]
63. Sen CK. Expanding Horizons of Cellular Plasticity in Regenerative Medicine. Am J Pathol. 2015; 185:2592–2595. [PubMed: 26435411]
64. Korns D, Frasch SC, Fernandez-Boyanapalli R, Henson PM, Bratton DL. Modulation of macrophage efferocytosis in inflammation. Front Immunol. 2011; 2:57. [PubMed: 22566847]
65. Filardy AA, Pires DR, Nunes MP, Takiya CM, Freire-de-Lima CG, Ribeiro-Gomes FL, DosReis GA. Proinflammatory clearance of apoptotic neutrophils induces an IL-12(low)IL-10(high) regulatory phenotype in macrophages. J Immunol. 2010; 185:2044–2050. [PubMed: 20660352]
66. Nucera S, Biziato D, De Palma M. The interplay between macrophages and angiogenesis in development, tissue injury and regeneration. Int J Dev Biol. 2011; 55:495–503. [PubMed: 21732273]
67. Rahat MA, Hemmerlein B, Iragavarapu-Charyulu V. The regulation of angiogenesis by tissue cell-macrophage interactions. Front Physiol. 2014; 5:262. [PubMed: 25071604]
68. Friedman EA. Advanced glycosylated end products and hyperglycemia in the pathogenesis of diabetic complications. Diabetes Care. 1999; 22(Suppl 2):B65–71. [PubMed: 10097902]
69. Huijberts MS, Schaper NC, Schalkwijk CG. Advanced glycation end products and diabetic foot disease. Diabetes Metab Res Rev. 2008; 24(Suppl 1):S19–24. [PubMed: 18442180]
70. McLellan AC, Thornalley PJ, Benn J, Sonksen PH. Modification of the glyoxalase system in clinical diabetes mellitus. Biochem Soc Trans. 1993; 21:158S. [PubMed: 8359411]
71. Dobler D, Ahmed N, Song L, Eboigbodin KE, Thornalley PJ. Increased dicarbonyl metabolism in endothelial cells in hyperglycemia induces anoikis and impairs angiogenesis by RGD and GFOGER motif modification. Diabetes. 2006; 55:1961–1969. [PubMed: 16804064]

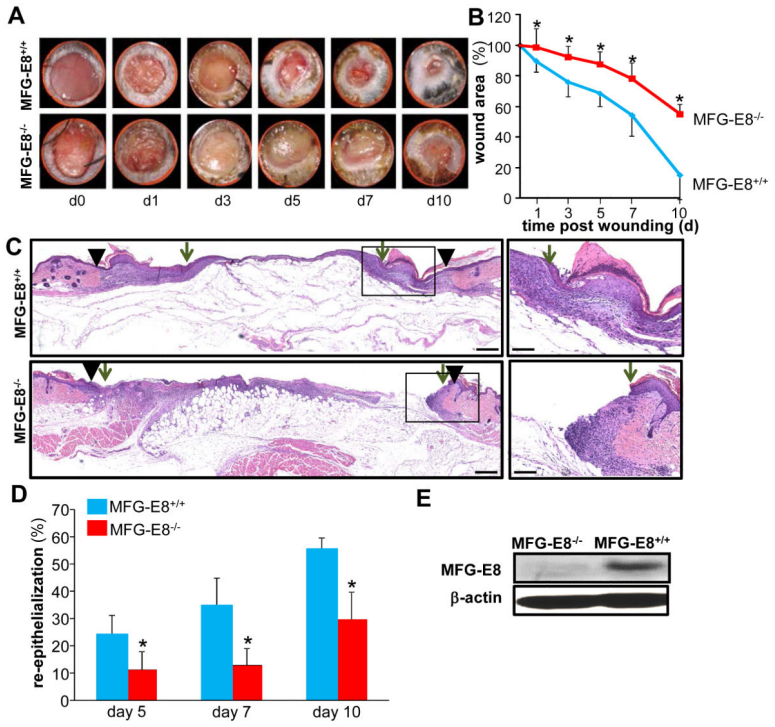

Figure 1. MFG-E8 deficiency impairs wound closure and wound re-epithelialization

A-D, Full-thickness (skin and panniculus carnosum) dorsal wounds were created on the male MFG-E8$^{-/-}$ and MFG-E8$^{+/+}$ mice by using a 6-mm biopsy punch. The wounds were stented and left to heal by secondary intention. Wounds were imaged on d0-10 post wounding. Wound areas were calculated using digital planimetry. **A,** Representative digital images of wounds from age matched MFG-E8$^{-/-}$ and MFG-E8$^{+/+}$ mice d0-10 post wounding. **B,** Wound closure kinetics. Data are expressed as mean ± SD (n=5); *p<0.05 compared to MFG-E8$^{+/+}$ wounds. **C,** Representative images of hematoxylin-eosin (H&E) stained d7 wound tissues. The wound edge is shown using solid black arrow heads and the wound epithelial margins shown by green arrows. **D,** Wound re-epithelialization calculated on d5, 7 and 10 post-wounding. Data are expressed as mean ± SD (n=3); *p<0.05 compared to MFG-E8$^{+/+}$ wounds. **E,** Western blot analysis of MFG-E8-L protein expression in skin from MFG-E8$^{+/+}$ and MFG-E8$^{-/-}$ mice. β-Actin was used as a loading control.

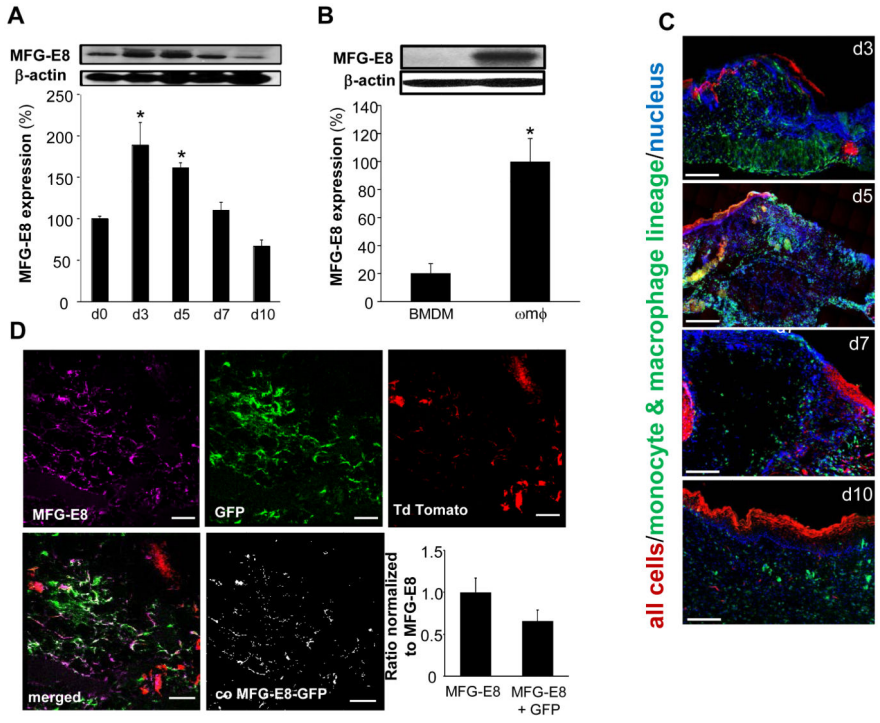

Figure 2. Macrophages are the primary source of MFG-E8 at wound-site in inflammatory phase

A, Western blot analysis of MFG-E8 protein expression in wound-edge tissues from C57bl/6 mice on d0-10 post wounding. β-Actin was used as loading control. Representative blot from four independent experiments has been provided. Densitometry quantification of the Western blot data was performed. Data is presented as % change compared to d0 (skin). Data are expressed as mean ± SD (n=4); *p<0.05 compared to d0 (skin). **B,** Western blot analysis of MFG-E8 protein expression in bone marrow derived monocytes (BMDM) and d3 wound mϕ (ωmϕ). β-Actin was used as a loading control. Representative blot from three independent experiments have been provided. Densitometry quantification of Western blot data has been presented. Data are expressed as mean ± SD (n=3); *p<0.05 as compared to BMDM. **C,** Representative images of wound-edge tissue sections d3-10 post wounding from ROSA-LysM mice displaying abundance of wound mϕ (GFP^+, green) at the wound-site peaked on d3 and 5 post-wounding. Most cells/tissue in these mice widely express cell membrane-localized red fluorescence, however, because of LysM driven cre recombinase only the cells of myeloid origin express membrane-localized green fluorescence. DAPI (blue, nuclear) staining was performed on wound tissue sections followed by fluorescence microscopy and imaging. Scale bar = 200μm. **D,** Representative images of d3 wound-edge tissue sections from ROSA-LysM mice stained with MFG-E8 (purple) to observe co-localization of MFG-E8 with green wound mϕ. The bar-graph represents the ratio of MFG-E8 that is contributed by macrophages (MFG-E8 co-localized with GFP positive macrophages) to the total MFG-E8 (purple) in field of view. The ratio of purple:green co-localization in confocal images was determined using automated unbiased co-localization module in FV10-ASW software (Olympus). Scale bar = 50μm. Bar-graph represents the fraction of MFG-E8 that is contributed by macrophages.

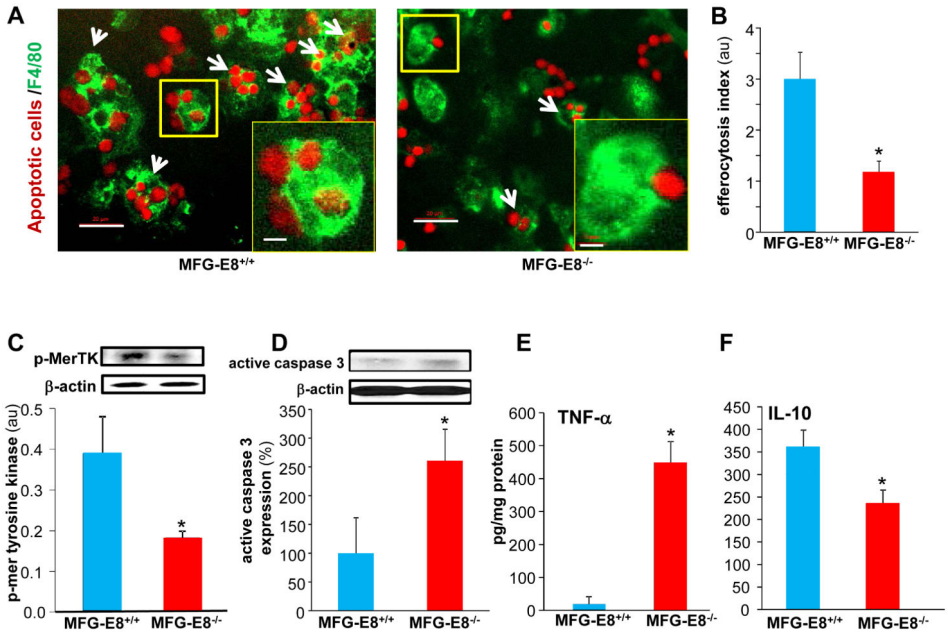

Figure 3. MFG-E8 supports efferocytosis and resolves inflammation at the wound-site

A-B, Efferocytosis activity in wound mϕ harvested from MFG-E8$^{-/-}$ and MFG-E8$^{+/+}$ mice. **A**, Representative images of wound mϕ (F4/80, green) co-cultured with apoptotic cells (pHrodo, red). White arrows points to mϕ that have engulfed two or more apoptotic cells. Scale bar = 20μm *Inset* Zoom of yellow box in the image showing a single mϕ engulfed apoptotic cells. Scale bar=5μm **B**, Efferocytosis index in d3 wound mϕ. Efferocytosis index is defined as the total number of engulfed apoptotic cells per mϕ present in a field of view. Data are expressed as mean ± SD (n= 3); *p<0.05 compared to MFG-E8$^{+/+}$ group. **C-D,** Western blot of **C**, MerTK phosphorylation in d3 wound mϕ following efferocytosis. **D**, active caspase 3 expression in d7 wound-edge tissues. β-Actin was used as a loading control. Representative blot from four independent experiments has been provided. Densitometry quantification of band intensity has been presented. Data are expressed as mean ± SD (n=4); *p<0.05 compared to MFG-E8$^{+/+}$ wound mϕ and wound-edge tissues respectively. **E-F,** Quantification of **E,** TNF-α and **F,** IL-10 measured by ELISA in the d7 wound-edge tissues. Data are expressed as mean ± SD (n=4); *p<0.05 compared to MFG-E8$^{+/+}$ wounds.

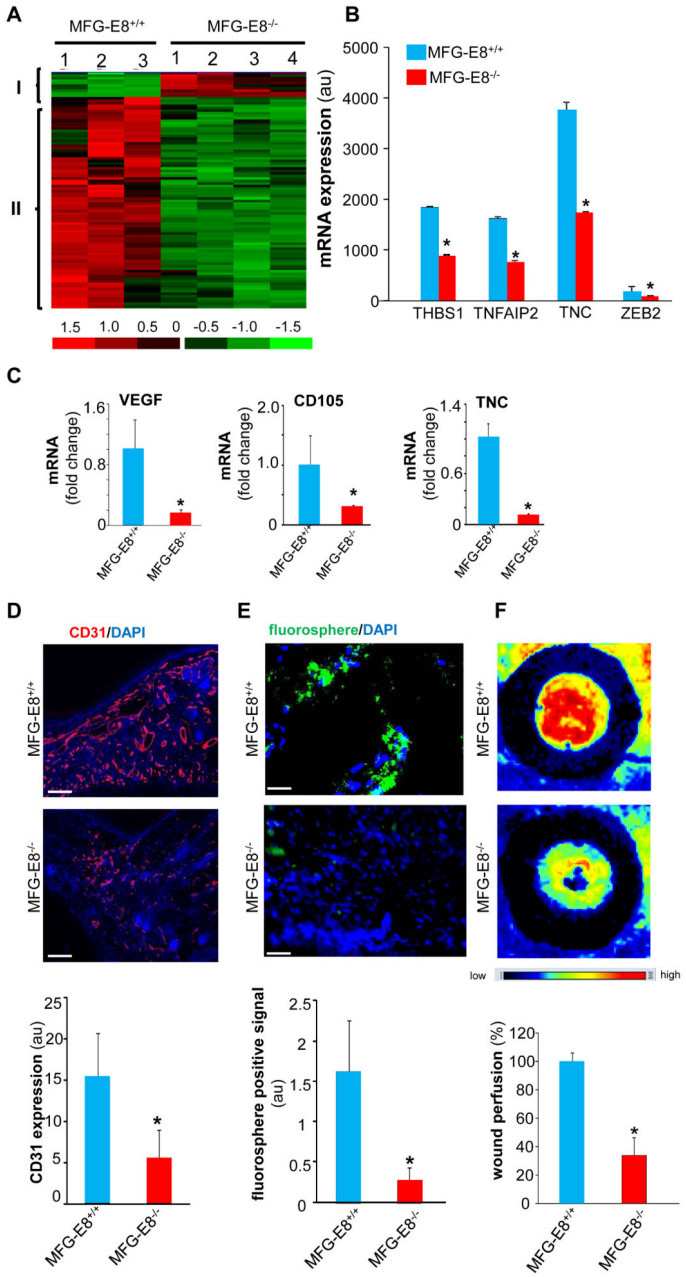

Figure 4. Impaired wound angiogenesis in MFG-E8$^{-/-}$ mice

A, All MFG-E8 sensitive transcripts in d5 wound-edge tissues were subjected to hierarchical clustering. **A**, Two major clusters of transcripts that were differentially ($p<0.05$; 2 fold or higher) regulated in MFG-E8$^{-/-}$ as compared to corresponding wild-type (MFG-E8$^{+/+}$) were identified. Red to green gradation in color represents higher to lower expression signal. A scale representing fold change is indicated at the bottom. **B,** Fold change of representative pro-angiogenic genes from microarray analysis has been presented. Data are expressed as mean ± SD (n=3); *$p<0.05$ compared to MFG-E8$^{+/+}$ wound-edge tissues. **C,** Expression levels of selected genes identified using GeneChip® analyses were independently determined using real-time quantitative (Q) PCR. Data are expressed as mean ± SD (n=3);

*p<0.05 compared to MFG-E8$^{+/+}$ wound-edge tissues. **D,** Representative images from CD31 (red) immunostained d5 wound-edge sections. The sections were counter stained with DAPI (blue, nuclear). Bar graph presents the quantification of CD31 positive areas of the d5 wound-edge tissues. Results are mean ± SD (n=3). *p < 0.05 compared to MFG-E8$^{+/+}$ wounds. Scale bar = 100μm. **E,** Representative images from space-filling carboxylate-modified green fluorescent microspheres injected mice to visualize wound vascularity. Sections were counterstained with DAPI (blue, nuclear). The appearance of the green microspheres in the wound-edge represents functional wound vascularity. Results are mean ± SD (n = 4). *p < 0.05 compared with MFG-E8$^{+/+}$ wound-edge tissues. Scale bar = 100μm. **F,** Laser Speckle images of d5 wounds. Bar graph represents the quantitative data from Laser Speckle analysis. Data presented as mean ± SD (n = 4); *p<0.05 compared to MFG-E8$^{+/+}$ wounds.

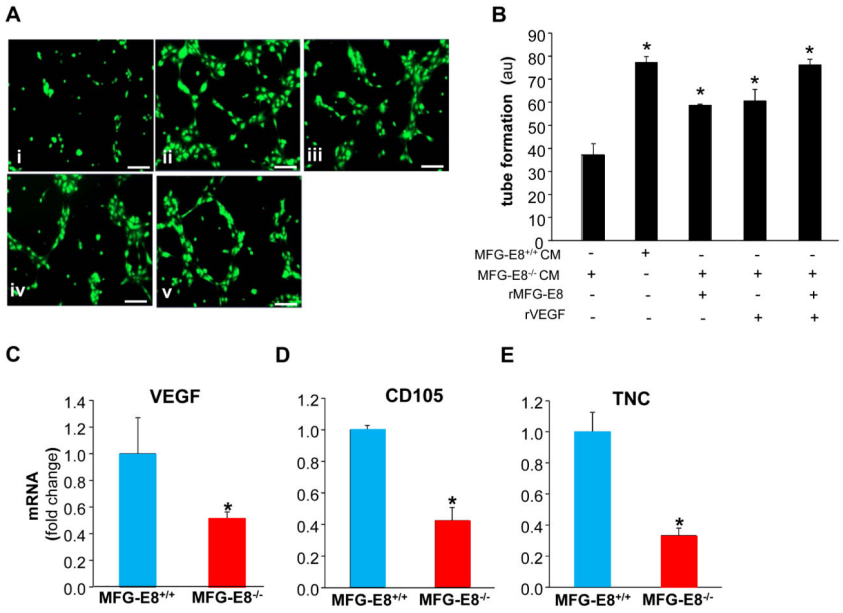

Figure 5. Wound macrophage derived MFG-E8 is angiogenic

A, Representative images of murine dermal endothelial cells (MDEC) subjected to Matrigel® assay. Following the assay, Calcein-AM (green) was used to stain and visualize the tube formation. The Matrigel® assay was performed in presence of conditioned media (CM) from d7 wound mϕ obtained from MFG-E8$^{-/-}$ and MFG-E8$^{+/+}$ mice. The CM was obtained by culturing freshly isolated wound mϕ 24h in a standard media. *i*, CM from MFG-E8$^{-/-}$; ***ii***, CM from MFG-E8$^{+/+}$; ***iii***, CM from MFG-E8$^{-/-}$ + rMFG-E8 (2.5μg); ***iv***, CM from MFG-E8$^{-/-}$ + VEGF (50ng); or ***v***, CM from MFG-E8$^{-/-}$ + rMFG-E8 (2.5μg) + VEGF (50ng). Scale bar = 100μm.**B**, Data presented in A was quantified and presented as bar graphs. Results are mean ± SD (n = 4). *$p < 0.05$ compared with cells treated with CM from MFG-E8$^{-/-}$ mice. **C,** Expression of specific pro-angiogenic genes in wound mϕ. The expressions were measured using real-time PCR. Results are mean ± SD (n = 3). *$p < 0.05$ compared with MFG-E8$^{+/+}$ wound mϕ.

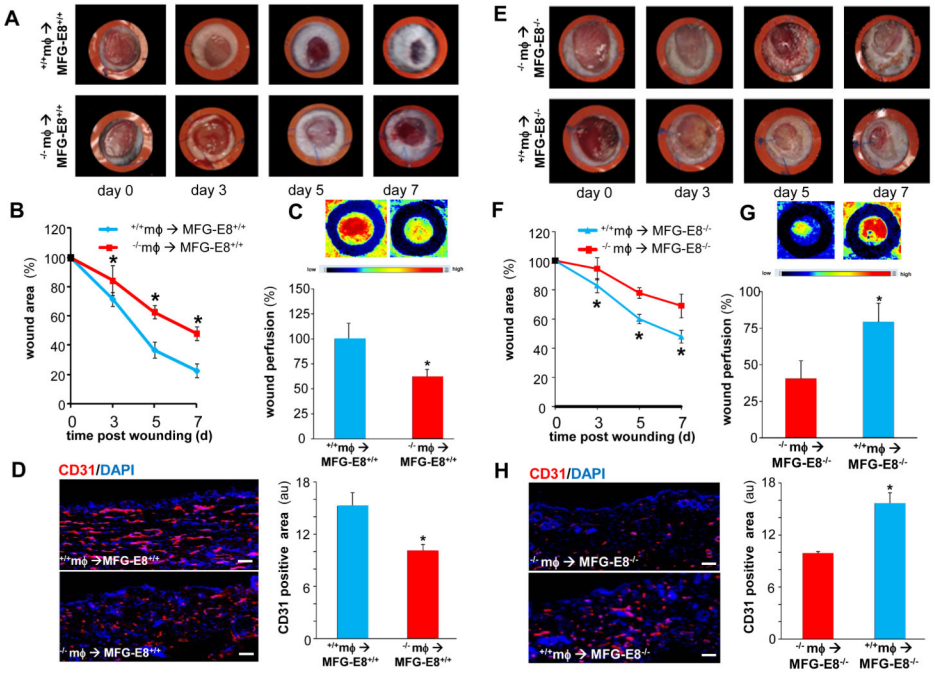

Figure 6. Rescuing MFG-E8 levels in the MFG-E8$^{-/-}$ mice wound macrophages using bone marrow transplantation improves wound angiogenesis and closure

Bone marrow chimera generation involved ablation of the bone marrow followed by reconstitution using the donor bone marrow either from MFG-E8$^{+/+}$ or MFG-E8$^{-/-}$ mice. **A-B,** full-thickness dorsal wounds were created using a 6-mm biopsy punch. The wounds were stented and left to heal by secondary intention. Wounds were imaged on d0-7 post wounding. **A,** Representative digital images of wounds of MFG-E8$^{+/+}$ mice that received MFG-E8$^{-/-}$ mϕ ($^{-/-}$ mϕ → MFG-E8$^{+/+}$) or MFG-E8$^{+/+}$ mice that received MFG-E8$^{+/+}$mϕ ($^{+/+}$mϕ → MFG-E8$^{+/+}$). **B,** Wound area measurements using digital planimetry. Data are expressed as mean ± SD (n=4). *p<0.05 as compared to $^{+/+}$mϕ → MFG-E8$^{+/+}$ mice. **C,** Laser speckle images of d5 wounds presented in A-B. Bar graph represents the quantitative data from Laser Speckle analysis. Data presented as mean ± SD (n = 4); *p<0.05 compared to $^{+/+}$mϕ → MFG-E8$^{+/+}$ mice. **D,** CD31 (red) immunostaining was performed in d5 wound-edge tissues. Bar graph represents the quantification of CD31 positive area. Results are mean ± SD (n = 4). *p < 0.05 compared with $^{+/+}$mϕ → MFG-E8$^{+/+}$ group. Scale bar = 50μm. **E,** Representative digital images of wounds of MFG-E8$^{-/-}$ mice that received MFG-E8$^{+/+}$ mϕ ($^{+/+}$ mϕ → MFG-E8$^{-/-}$) or MFG-E8$^{-/-}$ mice that received MFG-E8$^{-/-}$ mϕ ($^{-/-}$mϕ → MFG-E8$^{-/-}$). **F,** Wound area measurements using digital planimetry Data are expressed as mean ± SD (n=4). *p<0.05 as compared to $^{-/-}$mϕ → MFG-E8$^{-/-}$ mice. **G,** Laser speckle images of d5 wounds presented in E-F. Bar graph represents the quantitative data from Laser Speckle analysis. Data presented as mean ± SD (n = 4); *p<0.05 compared to $^{-/-}$mϕ → MFG-E8$^{-/-}$ mice. **D,** CD31 (red) immunostaining was performed in d5 wound-edge tissues. Bar graph represents the quantification of CD31 positive area. Results are mean ± SD (n = 4). *p < 0.05 compared with $^{-/-}$mϕ → MFG-E8$^{-/-}$ group. Scale bar = 50μm.

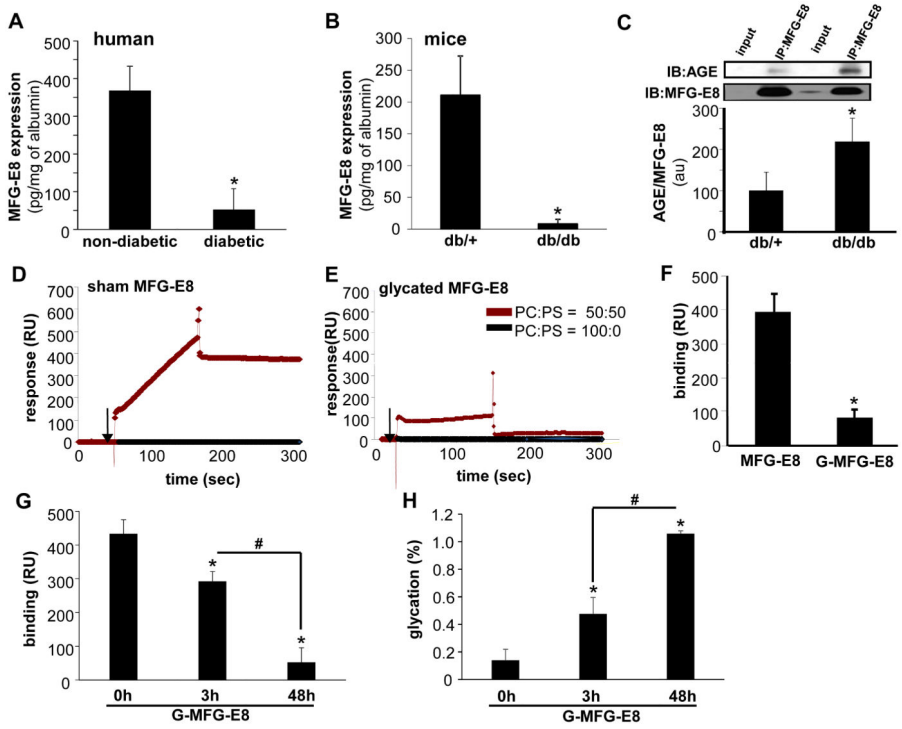

Figure 7. Lower MFG-E8 levels in the diabetic wound environment

A, MFG-E8 protein levels in the wound fluids (WF) obtained from diabetic and non-diabetic chronic wounds (see Table 1 for subject demographics). MFG-E8 levels were determined using ELISA. Results are mean ± SD (n = 5). *, $p < 0.05$ compared with non-diabetic WF. **B,** Hunt–Schilling wire mesh cylinders were implanted subcutaneously in the back of diabetic ($Lepr^{db}$, db/db) or corresponding non-diabetic controls (heterozygous, $Lepr^{db/+,}$ db/+) mice. WF were harvested d3 post-implantation, and MFG-E8 level in WF was determined using ELISA. Results are mean ± SD (n = 4). *, $p < 0.05$ compared to db/+ WF. **C,** Immunoprecipitation (IP) of MFG-E8 from day 3 wound edge tissue lysates of diabetic (db/db) or corresponding non-diabetic controls (db/+) mice. The IP was subjected to SDS–PAGE followed by immunoblotting (IB) with anti-AGE antibody. Input represents cell lysates after immunoprecipitation reaction. Results are mean ± SD (n = 4). *, $p < 0.05$ compared to db/+. **D-F,** Surface plasmon resonance (Biacore, SPR) assay. Binding affinity was tested using SPR with phosphotidylserine (PS) or phosphatidylcholine (control) liposomes immobilized on the sensor L1 chip and glycated MFG-E8 or sham MFG-E8 as soluble analytes. Glycation of MFG-E8 (G-MFG-E8) was achieved by incubating recombinant mouse MFG-E8 (10μg) with 10mM methylglyoxal (MGO) at 37°C for 48h while, sham MFG-E8 involved incubation with buffer at 37°C for 48h. The response curve of **D,** sham MFG-E8 or **E**, G-MFG-E8 binding with PS:PC (50:50) or PS:PC (0:100) liposomes has been presented. **F**, The quantification of the binding has been presented as bar graph. Results are mean ± SD (n = 3). *, $p < 0.05$ compared to sham MFG-E8. **G**, Dose dependent inhibition in binding affinity of G-MFG-E8 to PS as detected by Biacore SPR. The dose dependent glycation of MFG-E8 was achieved by incubating MFG-E8 at 37°C for 0, 3 and 48h. Results are mean ± SD (n = 3). *, $p < 0.05$ compared to 0h, $^{\#}$,$p < 0.05$ compared to 3h. **H**, Quantification of the level of glycation of MFG-E8 following 0, 3 or 48h

of exposure to MGO. The glycation of MFG-E8 was measured using glycoprotein carbohydrate estimation kit. Results are mean ± SD (n = 4). *, $p < 0.05$ compared to 0h; $^{\#}$, $p < 0.05$ compared to 3h.

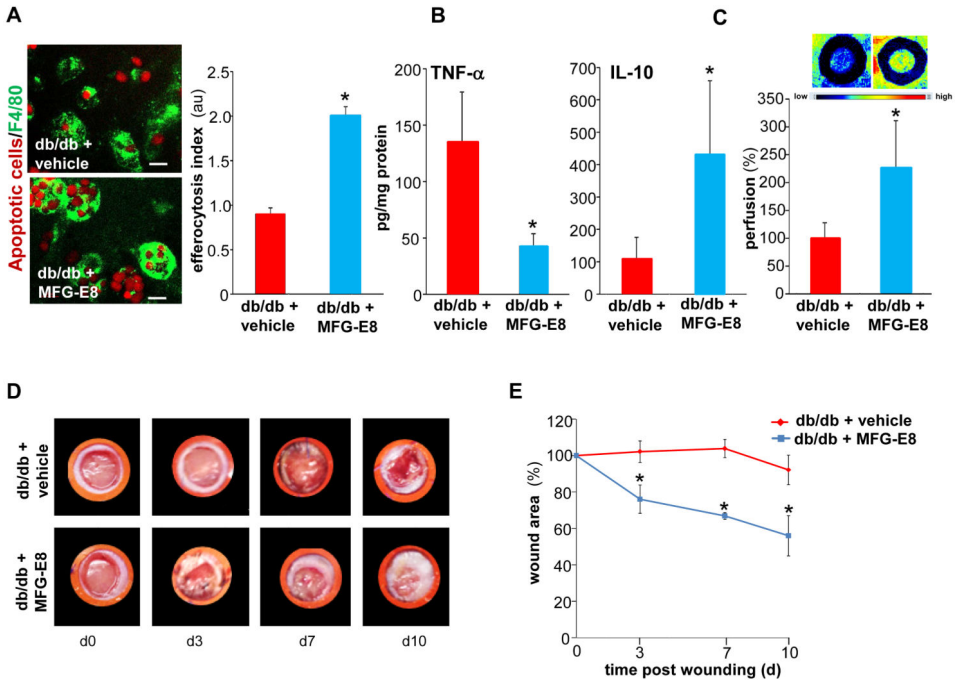

Figure 8. MFG-E8 treatment improves efferocytosis, angiogenesis and healing in diabetic wounds

A, Efferocytosis activity in d3 wound mϕ harvested from db/db animals. Freshly isolated wound mϕ were incubated with rMFG-E8 (1μg/ml) 2h prior to the subjecting them to efferocytosis in the presence of rMFG-E8 (1μg/ml) or vehicle. Representative images of mϕ (F4/80, green) co-cultured with apoptotic cells (pHrodo, red). Efferocytosis index was calculated and data presented as mean ± SD (n = 4); *p<0.05 compared to vehicle treated group. Scale bar = 10μm. **B-E,** Full-thickness dorsal wounds were created using a 6-mm biopsy punch on dorsal side of diabetic ($Lepr^{db}$, db/db) or corresponding non-diabetic controls (heterozygous, $Lepr^{db/+,}$ db/+) mice. The wounds were stented and left to heal by secondary intention. Each wound was either treated with either recombinant mouse MFG-E8 (1μg per wound in 50% glycerol/saline once daily) or equivalent amount of vehicle (mouse serum in 50% glycerine/saline once daily) for 10 days. **B**, Quantification of TNF-α and IL-10 measured by ELISA in the d10 wound-edge tissues. Data are expressed as mean ± SD (n=3); *p<0.05 compared to vehicle treated wounds. **C,** Laser Speckle images from d5 wounds. Bar graph presents quantification of the Laser Speckle analysis. Data presented as mean ± SD (n = 4); *p<0.05 compared to control mice. **D,** Representative wound images on d0-10 post wounding; **E,** Wound area measurements were done using digital planimetry. Data are expressed as mean ± SD (n=3). *p<0.05 as compared to vehicle treated db/db mice.

Table 1

Demographics characteristics of subjects used for wound fluid study

Parameter	Non-diabetic	Diabetic
Subjects (*n*)	**5**	**5**
Age	**49.6 ± 7.2**	**48.8 ± 1.2**
Males	**4**	**3**
Females	**1**	**2**
Race		
Caucasian	**4**	**3**
African American	**1**	**2**
Wound etiology		
pressure	**2**	**3**
surgical	**3**	**1**
unknown	**0**	**1**
Wound location		
abdominal	**1**	**1**
lower extremity	**4**	**4**